Research Article | Vol. 15, No. 10 / 1 Oct 2024 / Biomedical Optics Express 5947
Biomedical Optics EXPRESS

Development of a carboxymethyl chitosan functionalized slide for small molecule detection using oblique-incidence reflectivity difference technology

MENGJING XU,[1,2] BOYANG SHI,[3] HAOFENG LI,[1] XIAOHAN MAI,[1] LAN MI,[1] JIONG MA,[1] XIANGDONG ZHU,[4] GUOWEI WANG,[3,5] AND YIYAN FEI[1,2,6]

[1]*Department of Optical Science and Engineering, Shanghai Engineering Research Center of Ultra-Precision Optical Manufacturing, Key Laboratory of Micro and Nano Photonic Structures (Ministry of Education), School of Information Science and Technology, Fudan University, Shanghai 200433, China*
[2]*Quzhou Fudan Institute, 108 Minjiang Avenue, Kecheng District, Quzhou, Zhejiang Province, China*
[3]*State Key Laboratory of Molecular Engineering of Polymers, Department of Macromolecular Science, Fudan University, Shanghai 200433, China*
[4]*Department of Physics, University of California, One Shields Avenue, Davis, California 95616, USA*
[5]*gwwang@fudan.edu.cn*
[6]*fyy@fudan.edu.cn*

Abstract: Label-free optical biosensors have become powerful tools in the study of biomolecular interactions without the need for labels. High throughput and low detection limit are desirable for rapid and accurate biomolecule detection. The oblique-incidence reflectivity difference (OI-RD) technique is capable of detecting thousands of biomolecular interactions in a high-throughput mode, specifically for biomolecules larger than 1000 Da. In order to enhance the detection capability of OI-RD for small molecules (typically < 500 Da), we have developed a three-dimensional biochip that utilized carboxymethyl chitosan (CMCS) functionalized slides. By investigating various factors such as sonication time, protein immobilization time, CMCS molecular weight, and glutaraldehyde (GA) functionalization time, we have achieved a detection limit of 6.8 pM for avidin (68 kDa). Furthermore, accurate detection of D-biotin with a molecular weight of 244 Da has also been achieved. This paper presents an effective solution for achieving both high throughput and low detection limits using the OI-RD technique in the field of biomolecular interaction detection.

1. Introduction

Label-free optical biosensors have become powerful tools in the study of biomolecular interactions due to their ability to analyze biomolecular interactions without the need for labeling agents [1–4]. Two important factors for evaluating the performance of optical biosensors are throughput and limit of detection (LOD). High throughput (>10,000 per experiment) [5,6] allows optical biosensors to process a large number of samples, improving analysis speed and efficiency. Low LOD [7,8] enables optical biosensors to accurately detect molecules with low mass or at low concentrations, improving reliability and accuracy of detection. Therefore, optical biosensors with high throughput and low LOD are desirable.

Surface plasmon resonance (SPR) [9–11], bio-layer interferometry (BLI) [7,12,13], resonant waveguide grating (RWG) [14–16], and ellipsometry [17–19] are widely used label-free optical biosensors. Among these, SPR is recognized as the gold standard for studying biomolecular interactions, enabling real-time detection of shifts in resonance peaks due to refractive index changes near the metal surface. Commercial SPR-based biosensors can detect molecules with a

#534563 https://doi.org/10.1364/BOE.534563
Journal © 2024 Received 3 Jul 2024; revised 21 Aug 2024; accepted 3 Sep 2024; published 19 Sep 2024

Biomedical Optics EXPRESS

molecular weight as low as 100 Da [8]. Additionally, SPR is often combined with microfluidic chips to the simultaneously analyze several to dozens of samples [20]. BLI monitors biomolecular interactions by observing changes in the interference pattern of reflected light on the sensor surface, capable of detecting small molecules with a molecular weight as low as 129 Da [7]. When combined with 96-well microplates, they can process up to 96 samples simultaneously per run [12]. RWG utilizes waveguide resonance for real-time biomolecule interaction detection, directly detecting molecules with a molecular weight of 184 Da [14]. When coupled with microplates, it achieves a throughput of 384 detections in a single run [21]. Ellipsometry detects real-time changes in the polarization state of reflected light from sample surfaces, currently capable of directly detecting compounds with a minimum molecular weight of 201 Da [22]. When integrated with microarray chips, ellipsometry-based biosensors can achieve a single-run detection throughput of up to 2500. These sensors demonstrate remarkable sensitivity in detecting biomolecules with low molecular weight. However, they encounter a challenge in applications requiring high throughput, such as drug screening.

Oblique-incidence reflectivity difference (OI-RD) is an optical biosensor with the high throughput capability in biomolecular detection. It is a special ellipsometry-based technique that measures surface properties by detecting the differential reflectivity changes of p-polarized and s-polarized components [23–26]. By integrating with a microarray biochip, OI-RD is capable of detecting biomolecular interactions with a throughput of 14,000 per experiment [27]. However, OI-RD is not able to detect small molecules with a molecular weight less than 500 Da, as well as proteins at low concentrations.

Clearly, there is currently no optical biosensor that can simultaneously detect biomolecular interactions in high throughput and with low LOD. To address this challenge, we have developed a three-dimensional (3D) biochip that enhances the signal response of OI-RD, enabling its detection of biomolecular interactions in high throughput and with low LOD. The 3D biochip is created by epoxy slide functionalization with carboxymethyl chitosan (CMCS) as a scaffold and glutaraldehyde (GA) as a crosslinker. By optimizing sonication time, protein immobilization time, CMCS molecular weight, and GA functionalization time, we have achieved a LOD of 6.8 pM for avidin (68 kDa), which is approximately 44 times lower than that on two-dimensional epoxy chips. Furthermore, the 3D chip allows for the direct detection of D-biotin with a molecular weight of 244 Da, which is significantly smaller than the detection limit of 1765Da on the 2D epoxy chips. Based on the 3D biochip, OI-RD has demonstrated great potential for the detection of biomolecular interactions with high throughput and low LOD, which has promising applications in various fields.

2. Material and methods

2.1. Chemicals and reagents

Epoxy slides (75 mm × 25 mm × 1 mm, 91.9% transmittance) were purchased from Capital Bio Technology Co., Ltd (Beijing, China). Carboxymethyl chitosan (carboxymethylation at the C6 hydroxyl group, 150 and 500 kDa) was purchased from Oenrisi Chemical reagent Co., Ltd (Chengdu, China). Glutaraldehyde was obtained from Sangon Biotechnology Co., Ltd (Shanghai, China). D-biotin and Biotin-$(PEG)_6$-OH were procured from Aladdin Reagent (Shanghai, China). Biotin-NH-NH_2 was procured from Yuanye Biotechnology Co., Ltd (Shanghai, China). Bovine albumin (BSA), Biotinylated BSA (BBSA) were obtained from Sigma-Aldrich (Shanghai, China). Avidin and Biotin-PD14 were purchased from Thermo Fisher Scientific (Shanghai, China) and Dewing Biotechnology Co., Ltd (Shanghai, China), respectively. Deionized water was used in all experiments.

Biomedical Optics EXPRESS

2.2. Preparation of CMCS slides

To prepare CMCS slides, the commercial epoxy slides were immersed in a 3 wt% aqueous solution of CMCS, which was previously dissolved in water. The mixture was heated at 60 °C and stirred at 500 rpm for 48 hours. Subsequently, the slides were sonicated in deionized water to remove any excess CMCS. After sonication, the CMCS slides were dried using a nitrogen flow. They were then placed inside staining jars and stored at a temperature of 4 °C for future use.

To functionalize CMCS slides with GA, the slides were immersed in a stirred 25 wt% aqueous solution of GA at 50 rpm. After that, the slides were thoroughly cleaned with deionized water and dried with a nitrogen flow. Once dry, proteins were promptly printed onto the slides for OI-RD detection.

2.3. Characterizations of biochip

The static water contact angle was measured using a contact angle device from Shanghai Zhongchen Company (JC2000D1, China). Elemental characterization was performed using X-ray photoelectron spectroscopy (XPS) from Kratos (AXIS Kratos Supra+, UK).

2.4. Protein microarray printing

Proteins were dissolved in HEPES (pH 7.5) at a concentration of 0.5 mg/mL for printing using the Super Marathon printer (Arrayjet, UK). The proteins were printed onto epoxy, CMCS, and CMCS-GA slides in a 10-subarray format. Each subarray consisted of 8 × 8 spots. The printing was conducted at a temperature of 20 °C and a humidity of 50%. Each spot was printed with a single drop of sample, which had a volume of 100 pL. The distance between each spot was 300 µm. After printing, the slides were placed in a humidity chamber at room temperature for a minimum of 12 hours and then stored at 4 °C for future use.

2.5. OI-RD detection of biomolecular interactions

The diagram of OI-RD system is shown in Fig. 1(c). A 532 nm laser passes through a polarizer and a photo-elastic modulator (PEM) which modulates the polarization of the incident beam at a frequency of 50 kHz. The beam then passes through a phase shifter (PS) which introduces an adjustable phase difference between the *p*- and *s*-polarized components. The laser is then focused onto the rear surface of the slide and the reflected beams pass through a polarization analyzer. A slit is used to block the beam reflected from the front surface. The beam from the rear surface is then incident onto a photodiode converting the light into a voltage signal which is measured by lock-in amplifiers.

The measured OI-RD signal can be expressed as follows [28]:

$$\text{OI} - \text{RD signal} \cong \frac{4\pi\sqrt{\varepsilon_0}\varepsilon_2\cos\theta_0\sin^2\theta_0}{\varepsilon_1(\varepsilon_2\cos^2\theta_0 - \varepsilon_0\sin^2\theta_0)}\frac{(\varepsilon_1 - \varepsilon_2)(\varepsilon_1 - \varepsilon_0)}{\varepsilon_0 - \varepsilon_2}\frac{d}{\lambda} \tag{1}$$

where ε_0, ε_1, and ε_2 are the dielectric constants of the glass, protein, and the buffer, with values of 2.3, 2.0, and 1.7, respectively. Equation (1) shows that OI-RD signal can be maximized with incident angle θ_0 being equal to the Brewster angle which is 41.3° for the glass slide with $\varepsilon_0 = 2.3$. Since the noise level also increases rapidly with the incident angel close to the Brewster angle, θ_0 is set to be 37.2° in order to achieve a better signal-to-noise ratio. d is the thickness of the protein layer. Since the OI-RD signal is proportional to the protein thickness d, the use of a 3D biochip is capable of providing more space for protein immobilization, resulting in a larger OI-RD signal.

For microarray detection, OI-RD system also has a translation stage for horizontal scanning of the microarray, and a galvo scan lens for vertical scanning. It takes about 15 minutes to image the microarray.

Biomedical Optics EXPRESS

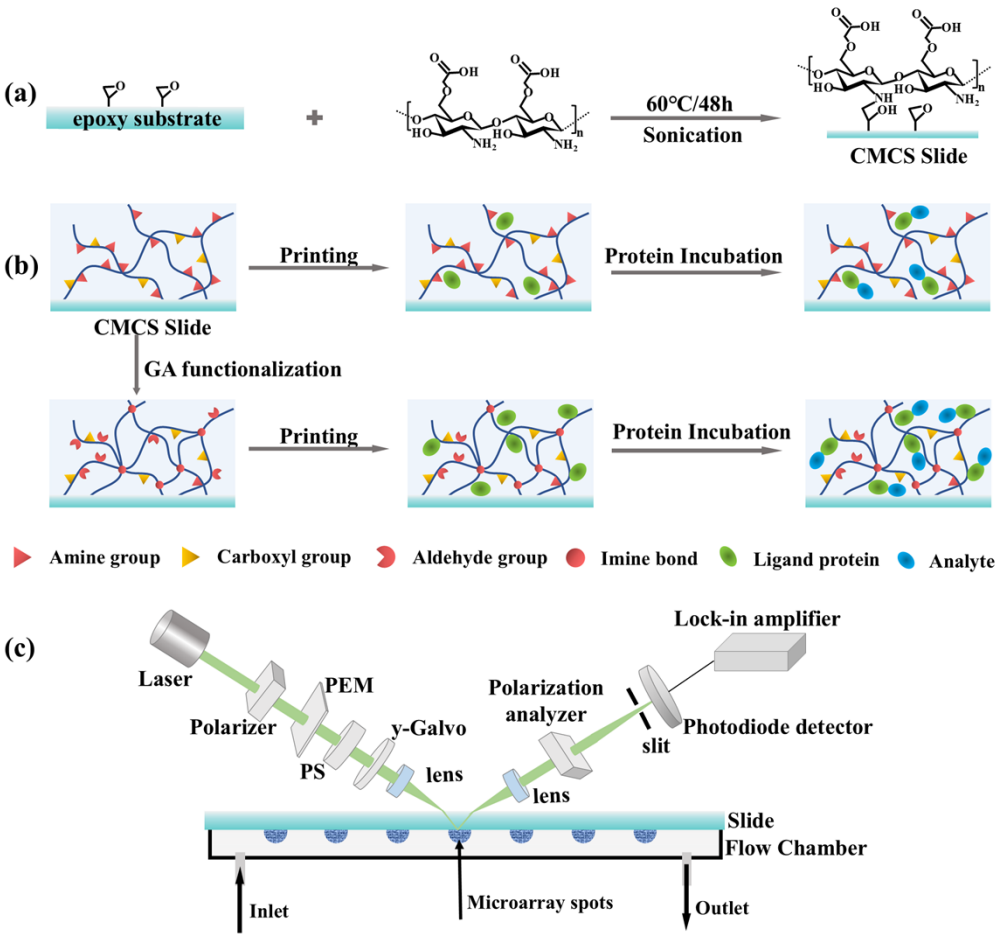

Fig. 1. (a) Schematic illustration of epoxy slide functionalization using CMCS. (b) Schematic illustration of biomolecule printing and incubation using CMCS slides. (c) Schematic diagram of the OI-RD system.

When imaging the biochip using the OI-RD platform, HEPES buffer was initially introduced into the fluid chamber to rinse off the proteins that were not immobilized on the slide. Next, the chip was blocked with a solution of 7.3 μM BSA in HEPES for 30 minutes. After the blocking step, the chip was incubated with the target protein for 1 hour. OI-RD images were captured both before and after each protein incubation step. The difference images, obtained by subtracting the pre-incubation images from the post-incubation images, were used for analysis. It took about 135 minutes to complete the detection of biomolecular interactions, including the scanning time for three OI-RD images, as well as 30 minutes for BSA blocking and 60 minutes for protein incubation.

To detect biomolecular interactions in real-time, unbound protein was first rinsed off the slide with buffer, followed by a 30-minute BSA (7.3 μM) blocking. Next, HEPES was introduced into the fluidic chamber at a rate of 0.01 mL/min for 10 minutes to establish a baseline signal. Then, the probe solution was injected into the fluidic chamber at a flow rate of 2 mL/min for 12 seconds, replacing the HEPES buffer. During the association phase, the probe was continuously flowed over the microarray at a rate of 0.01 mL/min for 33 minutes, allowing for biomolecular interactions. The dissociation phase began with a rapid flow of HEPES at a rate of 2 mL/min for

Biomedical Optics EXPRESS

12 seconds, followed by a 30-minute period of slow HEPES flow at a rate of 0.01 mL/min. The binding process was monitored in real-time by OI-RD, starting from the baseline and continuing until the dissociation was complete. It took about 148 minutes to complete the real-time detection of biomolecular interactions, which is 13 minutes longer than the end-point image detection. This is because the real-time monitoring process took about 73 minutes.

3. Results and discussion

3.1. Preparation and characterizations of 3D CMCS slides

To prepare 3D biochips, we used CMCS which is a polymer derived from carboxymethylation of chitosan. Chitosan is a natural polysaccharide and widely used in 3D functional biomaterial matrices [29–31]. CMCS offers improved solubility in deionized water compared to chitosan, due to the corporation of carboxyl groups into the chitosan structure. The epoxy slides were immersed in CMCS solutions with two different molecular weights, 150 kDa and 500 kDa, at a temperature of 60 °C for 48 hours. After removing excess CMCS by sonication in deionized water for 10 minutes, the slides were characterized using XPS and static water contact angle measurements.

XPS analysis was conducted on epoxy slide and two CMCS slides to investigate the changes in surface elements and functional groups resulting from the CMCS functionalization. Figure 2(a) shows the C1s spectra of the three slides. The peaks at 284.8 eV, 286.4 eV, and 288.1 eV, correspond to C-C, C-O/C-N, and C = O/O-C = O bonds, respectively [32,33]. It is clear that the peaks corresponding to C-O/C-N and C = O/O-C = O bonds become more significant with the introduction of CMCS of 150 kDa and 500 kDa. In addition, Fig. 2(b) shows that no characteristic peaks are observed for the epoxy slide in the N1s spectrum, while both CMCS slides exhibit distinctive peaks at 399.8 eV and 401.8 eV, corresponding to -NH_2 and -NH_3^+ groups, respectively [34,35]. These peaks indicate the presence of primary amine groups and partially protonated amine groups in CMCS. Together with the results of the C 1s spectrum, this suggests that CMCS has been successfully coated onto the surface of the epoxy slides.

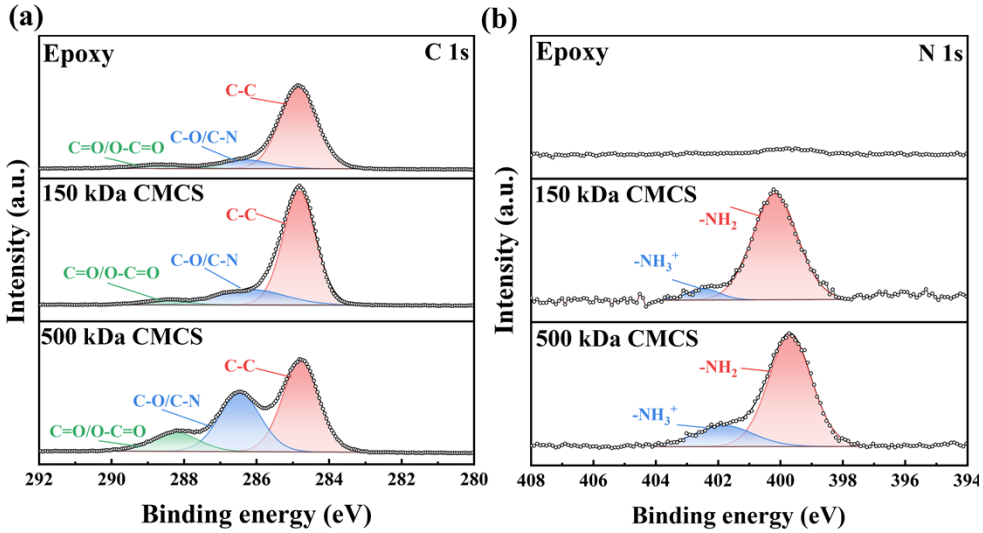

Fig. 2. (a) C 1s and (b) N 1s XPS spectra of epoxy slide and two CMCS slides.

Static water contact angle measurements were conducted on epoxy slides and CMCS slides. As shown in Fig. 3(a), the average contact angle for the 150 kDa CMCS slide is measured at

Biomedical Optics EXPRESS

35.1 ± 0.6°, while the 500 kDa CMCS slide exhibits an average contact angle of 41.9 ± 0.8°. In contrast, the epoxy slide displays an average contact angle of 56.9 ± 0.5°. It is clear that the surface of chitosan slide becomes more hydrophilic than epoxy slide, while the surface with coating of 500 kDa CMCS is slightly less hydrophilic than 150 kDa. This difference may be attributed to the inherent properties of CMCS, whereby an increase in the molecular weight of CMCS leads to a decrease in hydrophilicity [36–38].

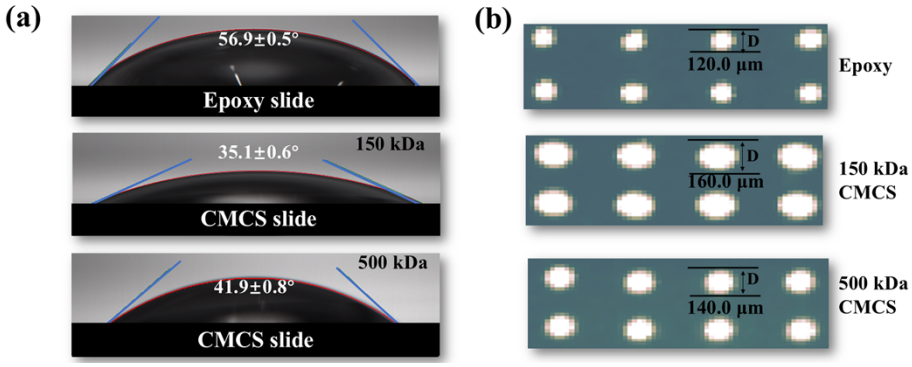

Fig. 3. (a) Static water contact angles of three slides. (b) Dimensions of printed protein spots on three slides measured by OI-RD.

The change in surface hydrophilicity through CMCS coating correlates with the observed variations in printed spot sizes, as shown in Fig. 3(b). In the OI-RD image of the printed BBSA protein microarray, the average diameter of BBSA spots on the epoxy slide is 120.0 µm, while those on 150 kDa and 500 kDa CMCS slides are 160.0 µm and 140.0 µm, respectively. Notably, the 150 kDa CMCS slide surface exhibits the smallest contact angle, which corresponds to the largest spot sizes, suggesting a highly hydrophilic slide surface. Conversely, the epoxy slide surface displays the largest contact angle, which corresponds to the smallest spot sizes, suggesting a less hydrophilic slide surface. The significant differences in contact angles and printed spot sizes between the CMCS slides and the epoxy slide provide evidence of the successful coating of CMCS polymer onto the epoxy slide.

Furthermore, we compared the performance of 3D CMCS slides with epoxy slides for the OI-RD detection of biomolecular interactions. We printed BBSA on the epoxy slide, as well as the 150 kDa CMCS slide and the 500 kDa CMCS slide. After printing BBSA on the epoxy and CMCS slides, the slides were placed in a refrigerator at 4°C for 40 hours, which was referred to as the "protein immobilization time". The slides were subsequently incubated with avidin at a concentration of 150 nM and detected using OI-RD. The binding amplitude between BBSA and avidin is approximately 5 mV on the epoxy chip (Fig. 4(a)), which increases to 16 mV on the 150 kDa CMCS slide (Fig. 4(b)), and further increases to 23 mV on the 500 kDa CMCS slide (Fig. 4(c)). This significant difference in protein binding amplitude between the CMCS slide and the bare epoxy slide provides further evidence of the successful coating the epoxy slide with CMCS polymer. In addition, it is evident that there is no direct correlation between the size of the microarray spots and the amplitude of OI-RD signals. This suggests that the impact of spot size variations on biomolecular interactions is insignificant compared to the influence of the biochip type. Finally, to clearly demonstrate the improvement in signal and reduce experimental discrepancies, we calculated the OI-RD signal ratio by dividing OI-RD signals obtained from 3D biochips by the average values obtained from the 2D epoxy slides. We found that the signal enhancement ratio for the 150 kDa CMCS slide is 3.2 (Fig. 4(d)), and for the 500 kDa CMCS slide is 4.6 (Fig. 4(f)).

Biomedical Optics EXPRESS

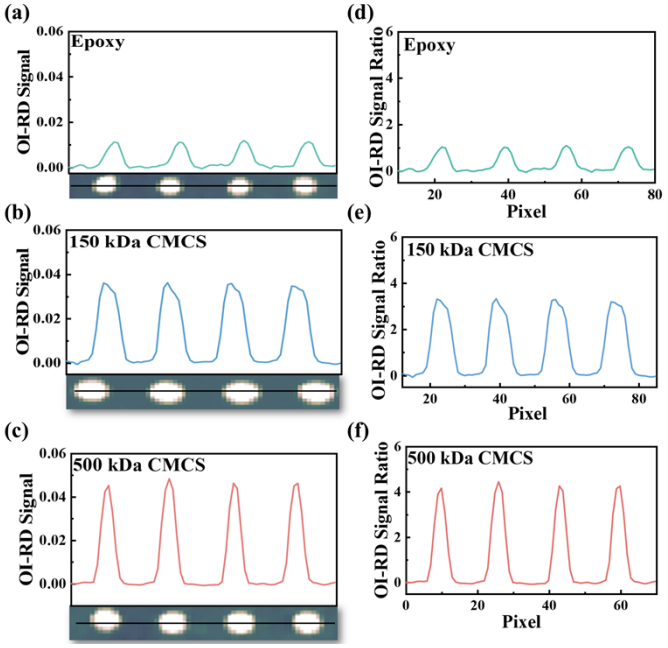

Fig. 4. The OI-RD signals between avidin and immobilized BBSA on (a) the epoxy slide, (b) the 150 kDa CMCS slide, and (c) the 500 kDa CMCS slide. OI-RD signal ratio for (e) the 150 kDa CMCS slide and (f) the 500 kDa CMCS slide compared to the (d) epoxy slide.

3.2. Effect of sonication time and immobilization time on signal enhancement

We then investigated experimental conditions to maximize OI-RD signal enhancement. We first studied the effect of sonication time on the OI-RD signal enhancement. The tested sonication time ranged from 10 to 200 minutes, with 10-minute increment. After each 10-minute sonication, the substrate was removed and rinsed with deionized water. The temperature in the sonication tank was kept constant throughout the sonication process. As shown in Fig. 5(a), as the sonication time increases, the OI-RD signal enhancement ratios for 150 kDa CMCS slide and 500 kDa CMCS slide remain stable around 3.2 and 4.5, respectively. This indicates that sonication does not remove CMCS from the slide surface. The stability of CMCS on the surface suggested that the CMCS was coated on epoxy slides by the covalent binding of amino groups on CMCS with epoxy groups on the slide surface [36–41]. Since prolonged sonication does not affect the signal enhancement, a sonication time of 10 minutes was used for the subsequent experiments.

We then investigated the impact of protein immobilization time on OI-RD signal enhancement by varying the protein immobilization time from 12 to 120 hours, as shown in Fig. 5(b). For the 150 kDa CMCS slide, as the immobilization time increases from 12 hours to 48 hours, the OI-RD signal enhancement ratio gradually increases from approximately 1.5 to 3.5. Subsequently, as the immobilization time further increases from 48 hours to 120 hours, the signal ratio levels off at around 3.5. For the 500 kDa CMCS slide, we observed a gradual increase in the OI-RD signal enhancement ratio from 4.5 to 6.5 as the immobilization period extends from 36 to 72 hours. For the immobilization time ranging from 72 to 120 hours, the enhancement ratio levels off at approximately 6.5. On the other hand, for the epoxy slide the OI-RD signal remains constant with the protein immobilization time ranging from 12 hours to 120 hours.

One obvious distinction among the three slides is the protein immobilization time to achieve the maximum OI-RD signal ratio. Specifically, the epoxy slide takes 12 hours, the 150 kDa CMCS slide takes 48 hours, and the 500 kDa CMCS slide takes 72 hours. The extended protein

Biomedical Optics EXPRESS

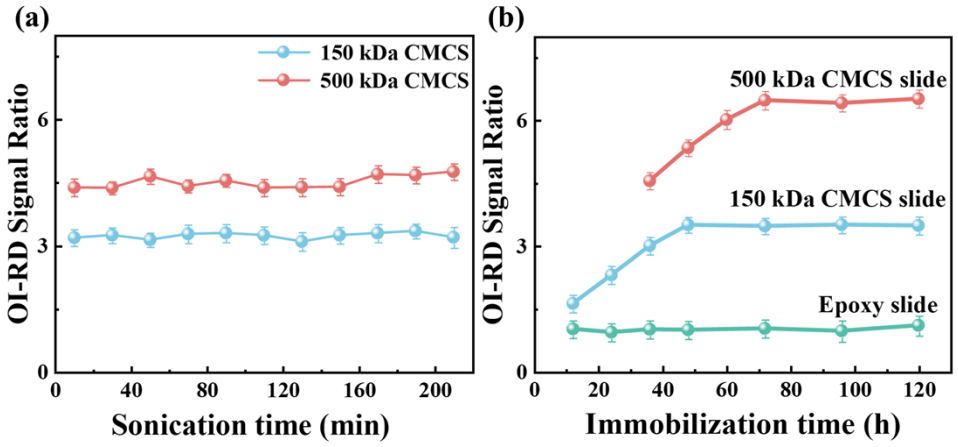

Fig. 5. (a) Effect of sonication time on OI-RD signal enhancement. (b) Effect of protein immobilization time on OI-RD signal enhancement.

immobilization time required for 150 kDa and 500 kDa CMCS slides to achieve maximal protein immobilization may be due to the need for sufficient time for the protein molecules to fully penetrate and immobilize within the 3D structure of CMCS formed through the staggered stacking of molecular chains [38]. Compared to the 150 kDa CMCS slides, a longer immobilization time is required to maximize the protein binding signal for 500 kDa CMCS slides. This could be due to the deeper 3D structure formed by the 500 kDa CMCS polymer, which requires proteins to diffuse for a longer period [36,37]. Thus, we selected a 48-hour immobilization time for 150 kDa CMCS slide and a 72-hour immobilization time for 500 kDa CMCS slide for the subsequent experiments.

Another obvious distinction among the three slides is the maximum OI-RD signal enhancement ratio. The 150 kDa CMCS slide achieves a maximum OI-RD signal enhancement ratio of 3.5, while the 500 kDa CMCS slide achieves a ratio of 6.5. This clearly demonstrates that the 3D structure of CMCS enhances the OI-RD signals by increasing the loading capacity compared to the 2D epoxy slide. In addition, it is expected that the proteins immobilized in the 3D structure will form non-covalent bonds through electrostatic adsorption or hydrophobic interaction [42,43] since the functional groups (-COOH, -OH, -NH_2) on CMCS are unable to efficiently form covalent bonds with proteins without a catalyst. Therefore, the OI-RD signal enhancement ratio for the 500 kDa CMCS slide is almost double that of the 150 kDa CMCS slide can be attributed to the larger loading capacity and increasing hydrophobic interactions between proteins and the polymer [44,45].

3.3. Effect of GA functionalization time on signal enhancement

To further enhance the OI-RD signal, we functionalized the CMCS slides with glutaraldehyde (GA). GA has two aldehyde functional groups, which serve two purposes. Firstly, it cross-links CMCS to form gel networks, creating a stable aqueous environment for protein interactions [46,47]. Additionally, it introduces aldehyde active sites for covalent bonding with proteins. The CMCS slides with relative molecular weights of 150 kDa and 500 kDa were immersed in a 25 wt% glutaraldehyde solution for a specific duration, referred to as the "GA functionalization time".

We then studied the effect of GA functionalization time on the enhancement of OI-RD signal. To optimal OI-RD signal, the protein immobilization time of the CMCS-GA slide was set to 144 hours. As shown in Fig. 6(a), the OI-RD signal enhancement ratio of 150 kDa CMCS-GA

Biomedical Optics EXPRESS

slides progressively increases from 6 to 12 as the GA functionalization time increases from 1 to 6 hours. When the functionalization time exceeds 6 hours, the OI-RD signal enhancement ratio starts to decrease, reaching a value of 9 with 24 hours of functionalization time. These findings demonstrate a significant enhancement of the OI-RD signal after GA functionalization. Additionally, the OI-RD signal decreases with increasing functionalization time beyond 6 hours, which may be attributed to steric hindrance and less effective avidin access due to excessive immobilization of BBSA, as demonstrated by Zhu et al [28]. Similarly, the 500 kDa CMCS-GA slide exhibited a comparable pattern, with the maximum signal ratio 19 occurring at 12 hours. This is attributed to the higher molecular weight of chitosan, which offers more reactive sites, necessitating a longer reaction time for glutaraldehyde to fully engage with it.

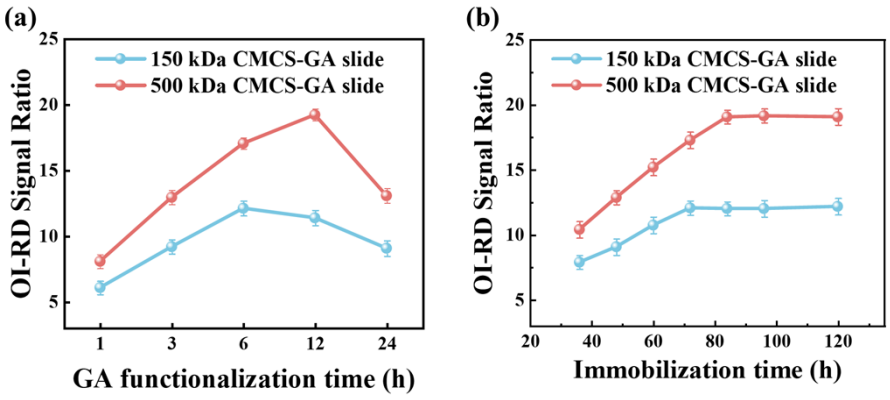

Fig. 6. (a) Effect of GA functionalization time on OI-RD signal enhancement for 150 kDa CMCS-GA slide. (b) Effect of immobilization time on OI-RD signal enhancement for 150 kDa CMCS-GA slide.

The effect of protein immobilization time on the OI-RD signal enhancement ratio was also investigated on the 150 and 500 kDa CMCS slides with a GA functionalization time of 6 and 12 hours, respectively (Fig. 6(b)). The results clearly demonstrate that the maximum achievable signal enhancement ratio on the 150 kDa CMCS-GA slide is 12, which is approximately 4 times higher than that on the 150 kDa CMCS slide. For the 500 kDa CMCS-GA substrate, the maximum signal enhancement is 19, which is about 3 times that of the CMCS substrate. In addition, it takes about 72 hours for the 150 kDa CMCS-GA slide and 84 hours for the 500 kDa CMCS-GA slide to reach the maximum signal enhancement, which is significantly longer than the 48 hours required for the 150 kDa CMCS slide and the 72 hours required for the 500 kDa CMCS slide. These differences in time could be attributed to the steric hindrance imposed by the gel structure of CMCS-GA formed through cross-linking. Given the optimal performance of the 500 kDa CMCS-GA chip, the next section will focus on characterizing the signal enhancement on the 500 kDa CMCS-GA slide by detecting proteins at low concentrations and biomolecules with low molecular weight, which generate small OI-RD signals.

4. LOD of the OI-RD technique based on the 3D biochip

By using a 500 kDa CMCS-GA slide, we conducted a study on the LOD of OI-RD technique for protein binding. The slide was functionalized with GA for 6 hours, followed by protein immobilization for 100 hours. BBSA was immobilized on the 3D gel slide, and then avidin was flowed over the BBSA at concentrations ranging from 1.5 nM to 0.015 nM. The real-time binding curves of BBSA with avidin at different concentrations are shown in Fig. 7(a). The two vertical dotted lines in the Fig. mark the beginning and end of the association phase, while the horizontal dotted line represents the zero amplitude. During the association phase, the OI-RD signals

Biomedical Optics EXPRESS

exhibit an almost linear increase with time, and the amplitudes at the end of the association phase are 2.69×10^{-2}, 1.26×10^{-2}, 7.3×10^{-3}, 2.8×10^{-3}, and 5×10^{-4} for avidin concentrations of 1.5, 0.75, 0.375,0.15, and 0.015 nM, respectively. Based on the Langmuir reaction model [48], we obtained the equilibrium dissociation constant (*Kd*) of 1.98×10^{-5} nM by globally fitting the five binding curves. The variations of OI-RD signal amplitude with avidin concentration are plotted in Fig. 7(b). Each amplitude and its corresponding error bar were calculated by averaging signals from 64 BBSA spots. It is evident that the OI-RD signal can be well fitted by a linear function within the investigated concentration range, with an R^2 value of 0.99889 [49]. The noise level σ of the OI-RD is approximately 1×10^{-4}. Therefore, using the 3σ definition [50], the LOD for OI-RD with the 3D gel biochip can be interpolated to be 6.8 pM for avidin.

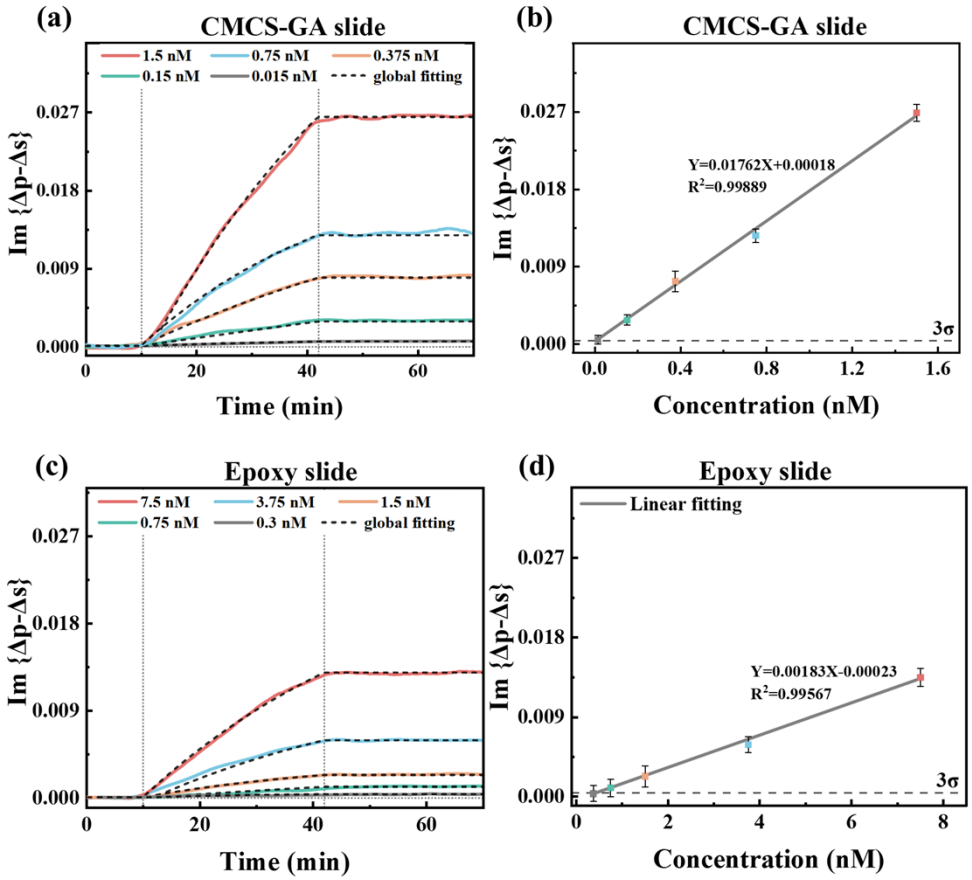

Fig. 7. (a) The real-time binding curves of BBSA with avidin at various concentrations on a 3D gel biochip. (b) Variations of OI-RD signal amplitude with avidin concentration on a 3D gel biochip. (c) The real-time binding curves of BBSA with avidin at various concentrations on a 2D epoxy biochip. (d) Variations of OI-RD signal amplitude with avidin concentration on a 2D epoxy slide.

Similar experiments were also conducted on a 2D epoxy slide, and the corresponding results are shown in Fig. 7(c), d. At an avidin concentration of 0.3 nM, the OI-RD signal is 3.5×10^{-4}. However, as the avidin concentration decreases further, the signals become too small to distinguish from the background. Using the 3σ definition, the LOD for avidin on the epoxy substrate is approximately 0.3 nM, which is about 44 times higher than the LOD for the 3D biochip.

Biomedical Optics EXPRESS

Next, we investigated the capability of the 500 kDa CMCS-GA 3D biochip to detect small molecules and determine the smallest detectable molecular weight. We performed experiments using avidin protein (7.3 μM in HEPES) printed on both the CMCS-GA 3D slide and the 2D epoxy slide. Biotin-labeled PD14 (100 nM), with a molecular weight of 1765Da, was then flowed over the avidin microarray. Figure 8(a) shows the OI-RD signals obtained for the binding of Biotin-PD14 to immobilized avidin. On the CMCS-GA 3D slide, the OI-RD signal is measured as 3.6×10^{-3}, which is more than 10 times higher than the signal obtained with the epoxy slide, approximately 3.2×10^{-4}.

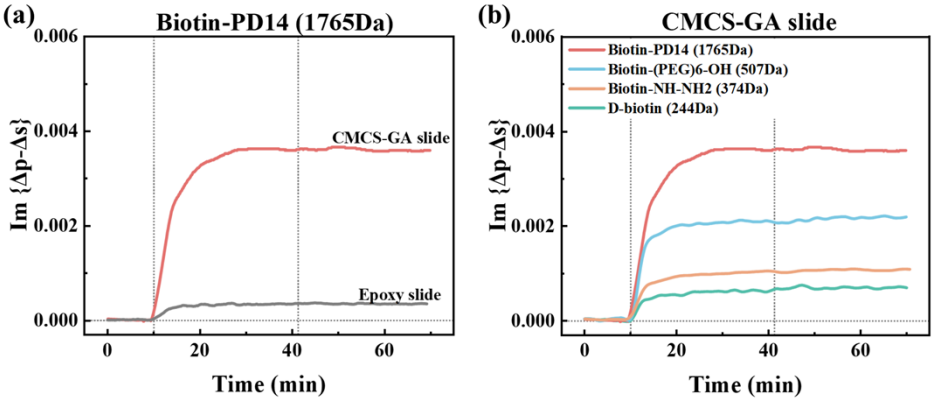

Fig. 8. (a) The real-time binding curves of Biotin-PD14 with avidin immobilized on CMCS-GA and epoxy slides. (b) The real-time binding curves of different molecular weights of biotin with avidin immobilized on CMCS-GA slide.

Furthermore, we conducted experiments using three other biotin molecules with molecular weights below 600 Da. All three were used at a concentration of 100 nM and flowed over avidin on both the CMCS-GA 3D slide and the 2D epoxy slide. On the epoxy slide, no OI-RD signals were observed for any of the three biotins. The binding curves of the three biotins to immobilized avidin on the CMCS-GA slide are shown in Fig. 8(b). For the analyte PD14 (1765Da), the OI-RD signal is 3.6×10^{-3}. The signals for Biotin-$(PEG)_6$-OH (507 Da) and Biotin-NH-NH_2 (374 Da) are 2.1×10^{-3} and 1.1×10^{-3}, respectively. Even for the D-biotin analyte with a molecular weight of 244 Da, the signal is approximately 6.2×10^{-4} and can still be distinguished from the background signal. Therefore, the CMCS-GA substrate allows for the detection of small molecules with a molecular weight equal to or greater than 244 Da. This is only 1/7 of the smallest biomolecular weight that can be detected on the epoxy slide.

5. Conclusion

In conclusion, we have successfully developed a 3D biosensor chip by functionalizing an epoxy slide with CMCS and further functionalizing it with GA. This has resulted in a lower LOD for OI-RD, compared to the commonly used 2D epoxy chip. On the optimized 3D slide, the LOD for direct detection of avidin is 6.8 pM, which is approximately 1/44 of that achieved with the epoxy slide. Additionally, the 3D biochip allows for the detection of D-biotin, with a molecular weight of 244 Da, which is approximately one seventh of that achievable with the epoxy slide. The combination of the ability to detect molecules at low concentrations and biomolecules with low molecular weight, along with the inherent high-throughput capacity, makes it possible to provide a biosensor that offers both high throughput and low LOD.

Funding. National Natural Science Foundation of China (32271510, 82030106, 62175036, 62175034); National Key Research and Development Program of China (021YFA0805200, 2021YFF0502900); Shanghai Key Laboratory of Metasurfaces for Light Manipulation (23dz2260100).

Biomedical Optics EXPRESS

Disclosures. The authors declare no conflicts of interest.

Data availability. Data underlying the results presented in this paper are not publicly available at this time but maybe obtained from the authors upon reasonable request.

References

1. S. Swami, F. Kayenat, and S. Wajid, "SPR biosensing: Cancer diagnosis and biomarkers quantification," Microchem. J. **197**, 109792 (2024).
2. R. Petersen, "Strategies using bio-layer interferometry biosensor technology for vaccine research and development," Biosensors **7**(4), 49–63 (2017).
3. Y. Fang, "Non-invasive optical biosensor for probing cell signaling," Sensors **7**(10), 2316–2329 (2007).
4. H. Liu, J. Shen, W. Liu, *et al.*, "Imaging ellipsometry biosensor: Basic theory, principles of operation, and applications," J. Vac. Sci. Technol., B **38**(2), 024002 (2020).
5. N. Berdigaliyev and M. Aljofan, "An overview of drug discovery and development," Future Med. Chem. **12**(10), 939–947 (2020).
6. A. Carnero, "High throughput screening in drug discovery," Clin Transl Oncol **8**(7), 482–490 (2006).
7. A. Vignon, A. Flaget, M. Michelas, *et al.*, "Direct detection of low-molecular-weight compounds in 2D and 3D aptasensors by biolayer interferometry," ACS Sens. **5**(8), 2326–2330 (2020).
8. R. Peltomaa, B. Glahn-Martínez, E. Benito-Peña, *et al.*, "Optical biosensors for label-free detection of small molecules," Sensors **18**(12), 4126 (2018).
9. R. D'Agata, N. Bellassai, V. Jungbluth, *et al.*, "Recent advances in antifouling materials for surface plasmon resonance biosensing in clinical diagnostics and food safety," Polymers **13**(12), 1929–1952 (2021).
10. D. Daems, J. Lu, F. Delport, *et al.*, "Competitive inhibition assay for the detection of progesterone in dairy milk using a fiber optic SPR biosensor," Anal. Chim. Acta **950**, 1–6 (2017).
11. Y. Wei, Y. Tang, Y. Zhang, *et al.*, "Wave type fiber SPR sensor for rapid and highly sensitive detection of hyperoside," Biomed. Opt. Express **15**(6), 3859 (2024).
12. V. Kamat and A. Rafique, "Designing binding kinetic assay on the bio-layer interferometry (BLI) biosensor to characterize antibody-antigen interactions," Anal. Biochem. **536**, 16–31 (2017).
13. S. Ouyang, B. Hu, R. Zhou, *et al.*, "Rapid and sensitive detection of nodularin-R in water by a label-free BLI aptasensor," Analyst **143**(18), 4316–4322 (2018).
14. Y.-C. Lin, W.-H. Hsieh, L.-K. Chau, *et al.*, "Intensity-detection-based guided-mode-resonance optofluidic biosensing system for rapid, low-cost, label-free detection," Sens. Actuators, B **250**, 659–666 (2017).
15. N. Zaytseva, J. G. Lynn, Q. Wu, *et al.*, "Resonant waveguide grating biosensor-enabled label-free and fluorescence detection of cell adhesion," Sens. Actuators, B **188**, 1064–1072 (2013).
16. Y.-T. Tseng, Y.-C. Chiu, V.-D. Pham, *et al.*, "Ultrasensitive upconversion nanoparticle immunoassay for human serum cardiac troponin I detection achieved with resonant waveguide grating," ACS Sens. **9**(1), 455–463 (2024).
17. S. Rafique, M. Idrees, H. Bokhari, *et al.*, "Ellipsometric-based novel DNA biosensor for label-free, real-time detection of Bordetella parapertussis," J. Biol. Phys. **45**(3), 275–291 (2019).
18. L. Liu, Y. -y. Chen, Y.-H. Meng, *et al.*, "Improvement for sensitivity of biosensor with total internal reflection imaging ellipsometry (TIRIE)," Thin Solid Films **519**(9), 2758–2762 (2011).
19. Y. Niu and G. Jin, "Protein microarray biosensors based on imaging ellipsometry techniques and their applications," Protein Cell **2**(6), 445–455 (2011).
20. E. Ouellet, C. Lausted, T. Lin, *et al.*, "Parallel microfluidic surface plasmon resonance imaging arrays," Lab Chip **10**(5), 581–588 (2010).
21. Y. Fang, "Label-free cell-based assays with optical biosensors in drug discovery," Assay Drug Dev. Technol. **4**(5), 583–595 (2006).
22. A. V. Nabok, A. Tsargorodskaya, A. K. Hassan, *et al.*, "Total internal reflection ellipsometry and SPR detection of low molecular weight environmental toxins," Appl. Surf. Sci. **246**(4), 381–386 (2005).
23. H. Zhang, M. Xu, H. Li, *et al.*, "Detection speed optimization of the OI-RD microscope for ultra-high throughput screening," Biomed. Opt. Express **14**(5), 2386–2399 (2023).
24. J. P. Landry, Y. Fei, X. Zhu, *et al.*, "Discovering small molecule ligands of vascular endothelial growth factor that block VEGF-KDR binding using label-free microarray-based assays," Assay Drug Dev. Technol. **11**(5), 326–332 (2013).
25. C. Zhu, R. Chen, Y. Zhu, *et al.*, "Calibration of oblique-incidence reflectivity difference for label-free detection of a molecular layer," Appl. Opt. **55**(33), 9459–9466 (2016).
26. J. P. Landry, Y. Fei, and X. Zhu, "Simultaneous measurement of 10,000 protein-ligand affinity constants using microarray-based kinetic constant assays," Assay Drug Dev. Technol. **10**(3), 250–259 (2012).
27. H. Li, M. Xu, X. Mai, *et al.*, "Analysis of fluid replacement in two fluidic chambers for oblique–incidence reflectivity difference (OI-RD) biosensor," Sensors **24**(6), 2000–2011 (2024).
28. J. P. Landry, Y. S. Sun, X. W. Guo, *et al.*, "Protein reactions with surface-bound molecular targets detected by oblique-incidence reflectivity difference microscopes," Appl. Opt. **47**(18), 3275–3288 (2008).
29. Z. Yaneva, D. Ivanova, N. Nikolova, *et al.*, "The 21st century revival of chitosan in service to bio-organic chemistry," Biotechnol. Biotechnol. Equip. **34**(1), 221–237 (2020).

Biomedical Optics EXPRESS

30. L. Upadhyaya, J. Singh, V. Agarwal, *et al.*, "The implications of recent advances in carboxymethyl chitosan based targeted drug delivery and tissue engineering applications," J. Controlled Release **186**, 54–87 (2014).
31. P. Rachtanapun, C. Rachtanapun, P. Jantrawut, *et al.*, (Ed.), *Multifaceted Carboxymethyl Chitosan Derivatives: Properties and Biomedical Applications*, (Springer Nature Switzerland, 2024), pp. 139–203.
32. W. M. E. M. M. Daniyal, Y. W. Fen, S. Saleviter, *et al.*, "X-ray photoelectron spectroscopy analysis of chitosan-graphene oxide-based composite thin films for potential optical sensing applications," Polymers **13**(3), 478–495 (2021).
33. R. S. Vieira, M. L. M. Oliveira, E. Guibal, *et al.*, "Copper, mercury and chromium adsorption on natural and crosslinked chitosan films: An XPS investigation of mechanism," Colloids Surf., A **374**(1-3), 108–114 (2011).
34. F. C. de Godoi, E. Rodriguez-Castellon, E. Guibal, *et al.*, "An XPS study of chromate and vanadate sorption mechanism by chitosan membrane containing copper nanoparticles," Chem. Eng. J. **234**, 423–429 (2013).
35. G. Lawrie, I. Keen, B. Drew, *et al.*, "Interactions between alginate and chitosan biopolymers characterized using FTIR and XPS," Biomacromolecules **8**(8), 2533–2541 (2007).
36. N. Chaiwong, P. Leelapornpisid, K. Jantanasakulwong, *et al.*, "Antioxidant and Moisturizing Properties of Carboxymethyl Chitosan with Different Molecular Weights," Polymers **12**(7), 1445 (2020).
37. M. Lei, W. Huang, J. Sun, *et al.*, "Synthesis, characterization, and performance of carboxymethyl chitosan with different molecular weight as additive in water-based drilling fluid," J. Mol. Liq. **310**, 113135 (2020).
38. M. Lei, W. Huang, Z. Jin, *et al.*, "Effect of molecular structure and ionization state on aggregation of carboxymethyl chitosan: A molecular dynamics study," Carbohydr. Polym. **297**, 119993 (2022).
39. A. Elizalde-Cárdenas, R. M. Ribas-Aparicio, A. Rodríguez-Martínez, *et al.*, "Advances in chitosan and chitosan derivatives for biomedical applications in tissue engineering: An updated review," Int. J. Biol. Macromol. **262**, 129999 (2024).
40. Z. Shariatinia, "Carboxymethyl chitosan: Properties and biomedical applications," Int. J. Biol. Macromol. **120**, 1406–1419 (2018).
41. L. Chen, Z. Tian, and Y. Du, "Synthesis and pH sensitivity of carboxymethyl chitosan-based polyampholyte hydrogels for protein carrier matrices," Biomaterials **25**(17), 3725–3732 (2004).
42. Y. Xu and Y. Du, "Effect of molecular structure of chitosan on protein delivery properties of chitosan nanoparticles," Int. J. Pharm. **250**(1), 215–226 (2003).
43. K. A. Janes, P. Calvo, and M. J. Alonso, "Polysaccharide colloidal particles as delivery systems for macromolecules," Adv. Drug Delivery Rev. **47**(1), 83–97 (2001).
44. M. Yahyaei, F. Mehrnejad, H. Naderi-manesh, *et al.*, "Protein adsorption onto polysaccharides: Comparison of chitosan and chitin polymers," Carbohydr. Polym. **191**, 191–197 (2018).
45. L. Bekale, D. Agudelo, and H. A. Tajmir-Riahi, "Effect of polymer molecular weight on chitosan–protein interaction," Colloids Surf., B **125**, 309–317 (2015).
46. Y. Y. Yeh, Y. T. Tsai, C. Y. Wu, *et al.*, "The role of aldehyde-functionalized crosslinkers on the property of chitosan hydrogels," Macromol. Biosci. **22**(5), 2100477 (2022).
47. P. Ramos, E. Chetrit, N. Yehuda, *et al.*, "Physical and antimicrobial properties of chitosan/silver nanoparticle composite hydrogels: role of the crosslinker," ACS Sustainable Chem. Eng. **11**(1), 133–143 (2023).
48. Y. S. Sun, J. P. Landry, Y. Y. Fei, *et al.*, "Effect of fluorescently labeling protein probes on kinetics of protein-ligand reactions," Langmuir **24**(23), 13399–13405 (2008).
49. Q. Hong, Y. Shen, S. Liu, *et al.*, "Re-examination of plotting analytical response against different forms of concentration," Anal. Chem. **93**(35), 11910–11914 (2021).
50. G. L. Long and J. D. Winefordner, "Limit of detection. A closer look at the IUPAC definition," Anal. Chem. **55**(07), 712A–724A (1983).